Surface plasmon mediated transmission of subwavelength slits at THz frequencies.

T. H. Isaac,[1] J. Gómez Rivas,[2] J. R. Sambles,[1] W. L. Barnes,[1] and E. Hendry[1]

[1]*School of Physics, University of Exeter,*

Stocker Road, Exeter, EX4 4QL, UK.

[2]*FOM Institute for Atomic and Molecular Physics,*

1098 SJ Amsterdam, The Netherlands.

Abstract

We present measurements and numerical modeling which elucidate the role of surface plasmons in the resonant transmission of a subwavelength slit in a conducting material. Using THz-time domain spectroscopy, we determine the Fabry-Perot transmission resonances for a single slit formed from a wafer of a semiconductor with a surface plasma frequency in the THz frequency range. We measure large red-shifts in the resonant frequencies close to the surface plasma frequency, approaching 50% lower than the resonance frequencies expected well below the surface plasma frequency, an effect attributed to the coupling of plasmons on the adjacent surfaces of the slit.
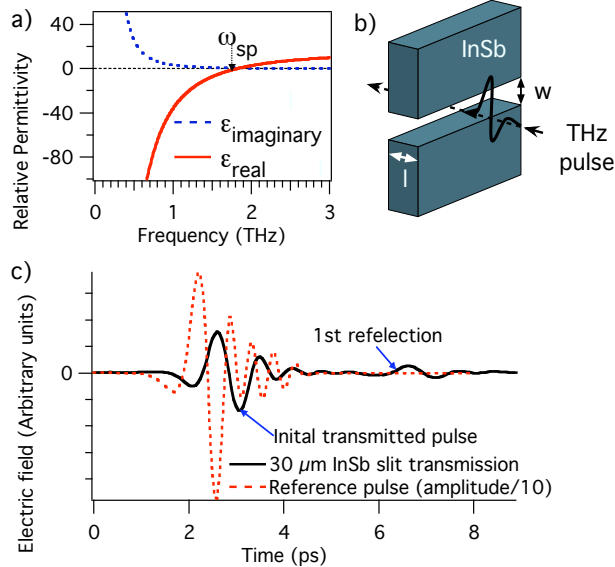
PACS numbers: 73.20.Mf, 42.79.Ag, 71.45.Gm, 78.20.Ci

FIG. 1: a)Drude modeled permittivity of InSb. ω_{sp} (for which $\epsilon_{real} = -1$) is indicated. b) Transmission of a THz pulse through an aperture defined by mechanically variable width w and fixed length l. c) Time domain electric field of a THz pulse measured in the far-field after transmission through a 30 μm wide aperture; the reflected pulse, which has made one round-trip of the slit length l is indicated. Also shown is the reference pulse, amplitude scaled down by a factor of 10.

The resonant transmission of radiation through a subwavelength slit in a screen of conducting material has recently been the subject of considerable theoretical[1–5], and experimental[6–8] work. For some time it has been known that narrow slits in metals at low frequencies support Fabry-Perot (FP) resonances, where an approximately half-integer number of wavelengths are quantized along the length of the slit. These quantized modes give rise to transmission resonances[9] of frequency ν_{fp} given by:

$$\nu_{fp} = \frac{nc}{2l} \tag{1}$$

where l is the length of the slit and n is an integer. For a slit in a slab of perfect metal (a material with infinite conductivity at all frequencies), it has been shown that Equation (1) provides an accurate estimate of the resonant transmission frequencies - provided that the slits are very narrow compared to the wavelength of the transmitted radiation[3,10].

However, for the case of narrow slits in real conductors with finite conductivity, the modes within the slits are coupled surface plasmons (SPs), and one obtains very large red-shifts[1,2] from the resonant transmission frequencies predicted by Eq. (1). Resonant slit cavities

feature in many photonic structures, many of which have potential applications, in sensing or spectroscopy[5,11,12]. It is therefore important to understand the role of SPs in influencing the resonant behavior of this fundamental system.

Here we present measurements and numerical modeling which elucidate the role of SPs in the transmission of subwavelength slits in conducting materials. Using THz-time domain spectroscopy (THz-TDS), we determine the behavior of FP transmission resonances for slits formed in wafers of Indium Antimonide (InSb), which has a surface plasma frequency (ω_{sp}) of around 1.7 THz. For narrow slits in the InSb we find that, near the surface plasma frequency, resonances are red-shifted by more than 50% from the values predicted by equation (1) - this frequency shift is more than two orders of magnitude larger than the shifts reported in metals at low frequencies[9]. By measuring the phase delay of the transmitted radiation we demonstrate that the coupling of SPs on the surfaces within the slit modifies the effective index of the mode within the cavity and hence the frequency of resonant transmission, an effect which becomes significantly stronger for frequencies approaching the surface plasma frequency.

Semiconductors have remarkably tunable dielectric functions. We choose a semiconductor with a surface plasma frequency in the THz range, so that the THz dielectric function is similar to that of metals at visible/ultraviolet frequencies. The dielectric function, $\epsilon(\omega)$, of InSb in this frequency region can be approximated using the Drude model:

$$\epsilon(\omega) = \epsilon_{lattice} - \frac{\omega_p^2}{\omega^2 + i\omega\gamma} \qquad (2)$$

In this model, $\epsilon_{lattice}$ is the zero frequency permittivity of the semiconductor, ω_p is the plasma frequency of the conductor and γ is the scattering frequency. In Fig. 1(a) we plot the room temperature dielectric function for typical InSb wafers using Drude parameters from the literature[13], with $\gamma \approx 0.8 \times 10^{12}$ radians/s and $\omega_p \approx 40 \times 10^{12}$ radians/s . Below we will refine the values of the Drude parameters for the samples of InSb used in our measurements.

Fig. 1(a) shows the large change in the dielectric function of InSb across the THz frequency range. The surface plasma frequency for a conductor-air interface is defined[14] as the frequency at which $\epsilon_{real} = -1$, and represents the high-frequency cut-off for a SP mode propagating on that interface[15]. The imaginary component of the dielectric function for InSb, which determines loss, is relatively small in this frequency range. In order to obtain ω_{sp} in the THz frequency range, other common semiconductors must be heavily doped. For

3

example, to obtain $\omega_{sp} = 2.0$ THz, for n-doped GaAs[16], $\omega_p = 45$ and $\gamma = 3.9$ radians/s. Similarly for n-doped Silicon[17] with $\omega_{sp} = 0.7$ THz, the Drude parameters are $\omega_p = 17$ and $\gamma = 5.2$ radians/s. In general, higher scattering rates will lead to SPs with shorter propagation length for a given surface plasma frequency.

The sample under investigation consists of a slit aperture in a wafer of undoped InSb with DC conductivity at 77K° of approximately 2400 Sm^{-1} and a thickness of 456 μm. The aperture is formed by cleaving a mono-crystalline wafer of InSb along a crystal plane using a diamond scribe. The two interfaces are aligned parallel to each other under a microscope, mounted on to micrometer translation stages so that the width w of the slit is variable and placed near the focus of a conical beam in a THz spectrometer. The resulting slit is defined by length l and width w - see Fig. 1(b). Under an optical microscope the sides of the slit are observed to be flat to within a few microns across its length.

The transmission of the slits is measured with incident THz radiation polarized normal to the slit. In general the polarization of the incident radiation must be TM with respect to the planes of top and bottom slit interfaces in order to excite SPs within the slit and observe resonant transmission; there are however some special cases in which TE modes can be supported within a subwavelength slit through inclusion of a high index dielectric material inside the cavity[18]. Here we only consider the case of air-filled slits with incident radiation polarized normal to the slit direction. All the slit sizes used are too small to support any TE cavity modes.

THz-TDS enables us to map out the electric field of a single-cycle THz pulse as a function of time, using a spectrometer similar to that reported in Ref.[19]. Briefly, THz pulses are generated through optical rectification[20] of 800 nm, 50 fs laser pulses in a 1 mm thick $\langle 110 \rangle$-oriented Zinc Telluride crystal, resulting in a THz pulse with bandwidth 0.1 - 3 THz. Detection is accomplished using a second identical ZnTe crystal by means of electro-optic sampling with the 800 nm laser pulses. The resulting time domain electric field profile (such as that plotted in Fig. 1(c)) can be converted to the frequency domain by means of a Fast Fourier Transform, yielding the complex electric field as a function of frequency, $E(\omega) = Ae^{i\phi}$. Because the measurements are fully time-resolved it is possible to extract both the amplitude A and phase ϕ of each frequency component. Normalized transmission intensities are found by dividing the spectral intensity transmitted through the sample by a free-space reference intensity; $T(\omega) = (A_{trans})^2/(A_{ref})^2$. We also calculate the effective
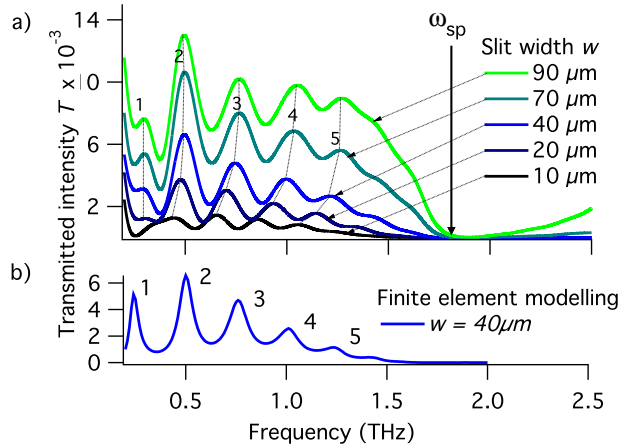
FIG. 2: a) Measured normalised transmission intensities for a slit in InSb for varying slit width w from 10-90 μm. Numbered peaks label the order of the corresponding FP-like transmission. b) Example of a finite-element modeled[21] spectrum through an InSb slit at $w = 40\mu m$

refractive index of the slit using the phase shift between reference and sample spectra, $\Delta\phi = \phi_{trans} - \phi_{ref}$, through the relation $n_{effective} = n_0 + \Delta\phi.c/\omega l$, where n_0 is the index of the reference medium (in this case air, $n_0 = 1$) and l is the length of the slit.

Time domain transmission through a slit in InSb is shown as Fig. 1(c). We firstly observe the initial THz pulse that is transmitted directly through the slit followed by a smaller time-delayed pulse - this is a reflected pulse that has made one round-trip of the slit. In Fig. 2(a) we plot the normalized intensity transmission spectrum as a function of frequency. The numbered transmission peaks on these figures indicate quantized FP peaks resulting from the cavity reflections. It should be noted that the first mode is at the very limit of the lowest measurable frequency for the THz spectrometer, and as such has a higher level of experimental error. Note that the observed peaks are considerably shifted from values predicted by Eq. (1). The first five FP modes are clearly observed, and the higher order peaks are seen to broaden and decrease in amplitude as they approach the surface plasma frequency. Measured transmission spectra agree well with those obtained from finite element modeling[21] of the system - an example of the modeled spectra is shown as Fig. 2(b). To obtain the best agreement between measurement and model we vary the InSb Drude parameters: the best fit is obtained with $\omega_p = 46 \times 10^{12}$ radians/s, and scattering frequency $\gamma = 0.63 \times 10^{12}$ radians/s. We take the lattice permittivity $\epsilon_{lattice}$ to be[22] 15.7. These values are comparable with published values[13,22] of InSb Drude parameters - any small
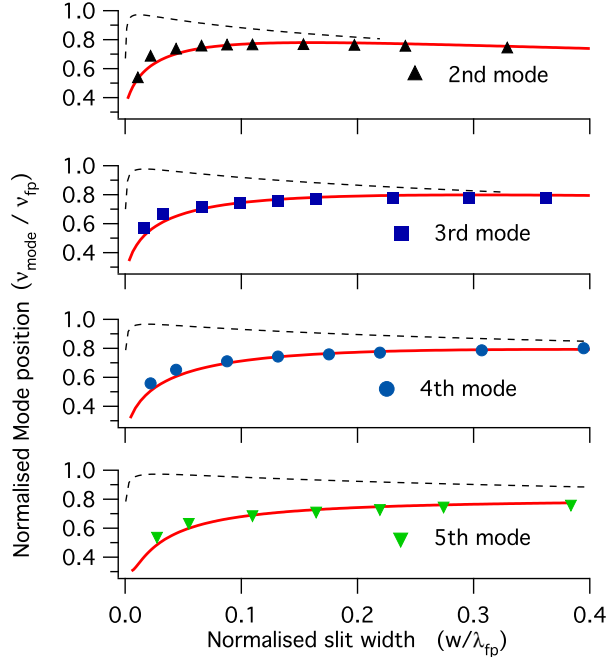
FIG. 3: Plot of normalized resonance frequencies, ν_{mode}/ν_{fp}, against normalised slit width, w/λ_{fp}, for modes 2 to 5 in an InSb slit. Solid lines are results of finite element modeling, markers are the results of measurements. The dashed lines show the results of finite element modeling of a slit with the same dimensions formed in aluminum.

deviation amongst reported values is readily accounted for by variation in impurity density between InSb samples.

On changing the width of the InSb slit aperture it is clear from the transmission spectra in Fig. 2(a) that the resonance peaks shift to lower frequency as the aperture width is decreased. In order to show the degree to which the frequency of each resonance moves, we plot in Fig. 3 the position of each resonance peak as a function of slit aperture size. The frequency of the peak position (ν_{mode}) is normalized to the corresponding FP frequency, given by Eq. (1) - we plot ν_{mode}/ν_{fp}. The slit width is scaled by the FP transmission wavelength (w_{slit}/λ_{fp}), giving a fully normalized plot that shows the fractional change in resonant frequency against the width of the slit compared to the resonance wavelength. Fig. 3 shows that the frequency of all the transmission resonances decreases for smallest slit widths, with measurements indicating shifts of around 50% from the frequencies predicted by Eq. (1) for slits of $w/\lambda_{fp} \leq 0.02$. The plot also illustrates a change in behavior between modes dependent on their proximity to the surface plasma frequency. Higher order modes,

6

with resonances closer to ω_{sp}, drop in frequency for slit widths which are a much larger fraction of the resonance wavelength. For example, the second order mode starts to decrease in frequency for normalized slit widths of $w/\lambda_{fp} < 0.16$, whereas the fifth order mode drops in frequency for slits of $w/\lambda_{fp} < 0.4$

For transmission of a slit in conducting material, there are two effects which give rise to shifts in the resonant frequencies from those predicted by Eq. (1). Firstly, it is known that the boundary conditions at the slit entrance and exit lead to a phase shift between light propagating inside the slit and the free-space radiation either side of it - an analytical formulation is given by Ref.[10]. This effect, which is important even for slits in highly conducting materials (i.e those materials with a surface plasma frequency considerably higher than the frequency of the incident light) results in an *decreasing* resonance frequency for increasing slit width[9,10] - this effect explains why ν_{mode}/ν_{fp} does not tend towards 1 for large slits in Fig. 3. A second effect arises from coupling of SPs on the internal interfaces of the slit[1,2,23], which gives rise to an increase in the effective index for the cavity mode, and therefore a *decrease* in resonance frequency for decreasing slit width. Approximate analytical expressions for this effect (which are valid in the case of $w \ll \lambda$) are given by Refs.[23] and[24]. It is clear from Fig 3 that the coupling of SPs has a pronounced effect on ν_{mode}/ν_{fp} for narrow slits.

Utilizing the phase-shift information $\Delta\phi$ of our measured THz spectra, we can plot in Fig. 4(a) the effective index for InSb slits, using the methods described above. First, for all the traces in Fig 4(a) we observe some small peaks in the effective index, corresponding to peaks in the transmission spectrum Fig. 2(a). These are due to the interference on resonance of directly transmitted light with light which has made at least one round trip of the slit cavity. More significantly there is a large change in the effective index near the surface plasma frequency. For smaller slit widths ($w \leq 20\mu m$), the effective index appears asymptotic to the surface plasma frequency - this behavior can be seen in the effective index plots for 10 and 20 μm slits shown in Fig. 4(a). For very small slits ($d \leq 20\mu m$) the transmitted intensity above the surface plasma frequency is very small, such that our phase measurements above ω_{sp} are erroneous. For larger slit widths ($w \geq 40\mu m$) the effective index returns to unity above the plasma frequency due to a small intensity of non-resonant transmission.

The transmission through a conducting slit in the limit of very narrow widths is mediated

by coupled SPs on the opposite sides of a conductor-insulator-conductor structure[24,25]. The complex propagation constant and, therefore, the effective index of refraction and the attenuation length of this mode can be calculated analytically. The results of these calculations are plotted as a function of frequency in Figs. 4(b) & 4(c) for different widths of the slit. Similarly to the measurements (Fig. 4(a)), the effective refractive index increases as the width of the slit is reduced and as the surface plasma frequency is approached from the low frequency side. This increase is due to greater penetration of the electromagnetic field into the conductor, which also causes the concomitant reduction of the SP propagation length due to ohmic losses. Though the agreement between the experiment and analytic model is not perfect (owing to defects inside the slit generated by sample machining which 'smear out' the measured phase-change). The calculations in Figs. 4(b) & 4(c) fully explain the general behaviour of the FP resonances on approaching the surface plasma frequency - the rapid change in effective index accounts for the shift in peak position, whilst the change in propagation length accounts for the broadening of the resonance peaks.

The coupling of SPs has been shown to play a role in determining the transmission of a conducting slit aperture even for frequencies well below the surface plasma frequency of the slit material (e.g aluminum at microwave frequencies[9]). For metals, surface plasma frequencies are typically in the UV region of the spectrum[22]. Using Finite Element modeling we compare the behavior of resonant transmission through our InSb slit to the behavior of an Aluminum slit of the same dimensions, across the same frequency range - the normalized resonance peak positions from this modeling are plotted as dashed lines in Fig. 3. The traces show that the position of each resonance in Aluminum slits does red-shift for very narrow slit widths. However the shift in Aluminum resonances occurs for much narrower slit widths than for the slits in InSb. Typically, the frequency drop is present in Aluminum slits for $w/\lambda_{fp} \leq 0.01$. These results can be compared to the measurements on the InSb slit, in which the fifth mode red-shifts for $w/\lambda_{fp} \leq 0.4$. This comparison emphasizes that near the surface plasma frequency of the slit material, resonance shifts due to coupling of SP modes occur for slits *more than two orders of magnitude larger* than for highly conducting materials.

In conclusion, we have elucidated the effect of coupled surface plasmons on the FP-like transmission of THz radiation through slits in conductors. For narrow slits we demonstrate that very large red-shifts in the resonant FP frequencies may be expected near the surface
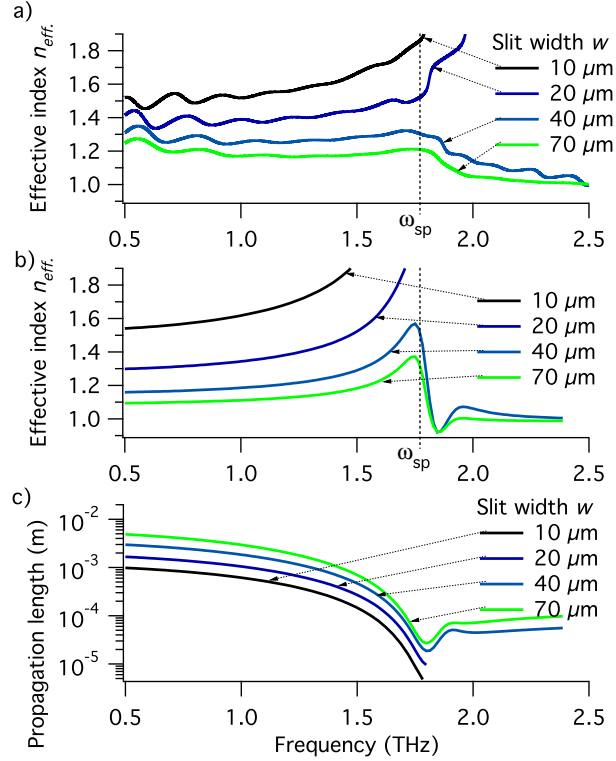
FIG. 4: a)The measured effective index of InSb slits with aperture widths w from 10 to 70 μm. The effective index of the 10 and 20 μm slits increases rapidly approaching the surface plasma frequency. b) Theoretically calculated values of the effective index of InSb slits of varying width w. c) The calculated propagation length of the coupled SP inside the InSb slits for various slit widths w.

plasma frequency, an effect attributed to the coupling of surface plasmons on the adjacent interfaces of the slit. These shifts must be accounted for in the design of devices that make use of resonant slit cavities, especially those in conductors close to the surface plasma frequency.

[1] J. A. Porto, F. J. García-Vidal, and J. B. Pendry, Physical Review Letters **83**, 2845 (1999).

[2] R. Gordon, Physical Review B **73**, 153405 (2006).

[3] Y. Takakura, Physical Review Letters **86**, 5601 (2001).

[4] R. Parthasarathy, A. Bykhovski, B. Gelmont, T. Globus, N. Swami, and D. Woolard, Physical Review Letters **98**, 153906 (2007).

[5] J. Bravo-Abad, L. Martín-Moreno, and F. J. García-Vidal, Physical Review E **69**, 026601 (2004).

[6] F. J. García-Vidal, H. J. Lezec, T. W. Ebbesen, and L. Martín-Moreno, Physical Review Letters **90**, 213901 (2003).

[7] Z. Sun, Y. S. Jung, and H. K. Kim, Applied Physics Letters **83**, 3021 (2003).

[8] J. W. Lee, M. A. Seo, D. S. Kim, S. C. Jeoung, C. Lienau, J. H. Kang, and Q.-H. Park, Applied Physics Letters **88**, 071114 (2006).

[9] J. R. Suckling, A. P. Hibbins, M. J. Lockyear, T. W. Preist, J. R. Sambles, and C. R. Lawrence, Physical Review Letters **92**, 147401 (2004).

[10] R. F. Harrington and D. T. Auckland, IEEE Transactions on Antennas and Propagation **AP-28**, 616 (1980).

[11] D. Crouse and P. Keshavareddy, Optics Express **13**, 7760 (2005).

[12] Y. S. Jung, Z. Sun, J. Wuenschell, H. K. Kim, P. Kaur, L. Wang, and D. Waldeck, Applied Physics Letters **88**, 243105 (2006).

[13] S. C. Howells and L. A. Schlie, Applied Physics Letters **69**, 550 (1996).

[14] H. Raether, *Surface Plasmons on Smooth and Rough surfaces and on Gratings* (Springer-Verlag, 1988).

[15] F. Yang, J. R. Sambles, and G. W. Bradberry, Physical Review B **44**, 5855 (1991).

[16] P. G. Huggard, J. A. Cluff, G. P. Moore, C. J. Shaw, S. R. Andrews, S. R. Keiding, E. H. Linfield, and D. A. Ritchie, Journal of Applied Physics **87**, 2382 (2000).

[17] T.-I. Jeon and D. Grischkowsky, Physical Review Letters **78**, 1106 (1997).

[18] D. Crouse and P. Keshavareddy, Optics Express **15**, 1415 (2007).

[19] A. Nahata, A. S. Weling, and T. F. Heinz, Applied Physics Letters **69**, 2321 (1996).

[20] M. Bass, P. A. Franken, J. F. Ward, and G. Weinreich, Physical Review Letters **9**, 446 (1962).

[21] *HFSS version 10*, Ansoft Corporation, Pittsburgh (2006).

[22] E. D. Palik, ed., *Handbook of Optical Constants of Solids* (Academic Press, 1985).

[23] S. Collin, F. Pardo, and J.-L. Pelouard, Optics Express **15**, 4310 (2007).

[24] S. I. Bozhevolnyi and T. Søndergaard, Optics Express **15**, 10869 (2007).

[25] E. N. Economou, Physical Review **182**, 539 (1969).